



ON THE GAUSS-SHAPED DIPOLE ANTENNA ABOVE A GROUND PLANE OF FINITE EXTENT

AUTHORS:

A. A. Ayorinde¹, S. A. Adekola² and I. Mowete^{3,*}

AFFILIATIONS:

^{1,2,3}Department of Electrical and Electronics Engineering, University of Lagos, Akoka, Lagos, Nigeria.

*CORRESPONDING AUTHOR:

Email: amowete@unilag.edu.ng

ARTICLE HISTORY:

Received: 30 July, 2024.

Revised: 18 November, 2024.

Accepted: 28 November, 2024.

Published: 31 December, 2024.

KEYWORDS:

Gauss dipole, Landstorfer antenna, Finite ground plane, Front-to-back ratio, Return loss.

ARTICLE INCLUDES:

Peer review

DATA AVAILABILITY:

On request from author(s)

EDITORS:

Chidozie Charles Nnaji

FUNDING:

None

Abstract

This paper investigates the influence of finite ground plane shape and size on the performance characteristics of a thin-wire antenna, whose shape is defined by the normal (Gaussian) probability distribution geometry, and which has been referred to in the literature as the “Gauss-shaped dipole antenna”. In the moment-method (MoM) formulation and solution utilized in the paper for a 1.5λ Gauss dipole antenna, the three candidate ground plane shapes considered, namely; square, rectangular, and circular, are modelled by wire-grids. Among a few other interesting properties, the computational results obtained indicate that both maximum achievable power gain and return loss depend on ground plane shape, emerging respectively, as (25.36dB, 47.28dB) for the circular shape; (15.81dB, 27.57dB), for the square shape, and (19.7dB, 34.32dB) for the rectangular shape. The results also reveal that ground plane sizes exhibit significant influence on the antenna’s performance metrics, and support the important conclusion in the literature that for the finite-ground-plane backed Gauss-shaped dipole antenna, one limitation is a characteristic gain / front-to-back- ratio trade-off.

1.0 INTRODUCTION

Research interest in the optimum-shaped wire dipole antenna may be said to have received impetus from the pioneering contributions of Landstorfer [1]. As remarked in [2], the analytical and experimental investigations of that pioneering contribution established that in terms of maximum achievable directivity, the 1.5λ long ‘Gauss-shape’ represents the optimum shape for the thin-wire dipole antenna. Notable analytical support for the theoretical expositions in [1] was provided by Cheng and Liang, [3], who, by eliminating the assumption of a sinusoidally distributed current flow imposed in [1], and using piece-wise parabolic segments for initial shape approximation, optimized antenna shape for maximum directivity. That contribution rigorously demonstrated that the Gauss-shaped dipole (GSD) provides maximum achievable gain. Quite a few other wire antenna shape optimization problems have also been since addressed in the literature. These include the curved-surface dipole shape optimization problem described by [4], in which investigations focused on identifying the geometrical parameters of Gauss-curved and V surface dipoles, that will yield maximum directivity. Kataja, [5] defined a shape optimization problem as that of determining the

Vol. 43, No. 4, December 2024

HOW TO CITE:

Ayorinde, A. A., Adekola, S. A., and Mowete, I. “On the Gauss-Shaped Dipole Antenna above a Ground Plane of Finite Extent”, *Nigerian Journal of Technology*, 2024; 43(4), pp. 696 – 705; <https://doi.org/10.4314/njt.v43i4.10>

© 2024 by the author(s). This article is open access under the CC BY-NC-ND license

dipole, whose size and optimum shape correspond to a prescribed input impedance, at the center frequency. One important outcome reported in [5] is that the optimally directive 1.5λ planar dipole has identical performance characteristics as the optimal directive 1.5λ non-planar dipole. A somewhat similar problem presented in [6], considered the simultaneous optimization of input impedance and directivity as the objective of the shape optimization problem. On the other hand, two different shape optimization problems addressed by the contributions in [7] and [8] limited considerations, in the case of [7], to the determination (for a wire antenna of finite thickness) of normalized antenna length and radius, for which antenna input impedance emerges as a pre-specified value; whereas, Wang, Jen and Jiang [8], addressed the problem of the antenna shape, optimized for maximum peak values of radiated pulse.

In all the representative contributions mentioned in the foregoing discussions, reported maximum achievable directivity (or gain, in some cases) ranged from 7.0 dB [5] through 7.132dB [3], to 7.198 dB [6]. It is not surprising therefore, to find that majority of the curvilinear wire dipole array-based gain improvement schemes presented in the literature, utilized GSDs as array elements. The more prominent of such schemes include the log-periodic configuration described in [2], for which a remarkably high gain performance was reported. Following the analytical procedure developed in [3], Liang and Cheng [9], in another notable contribution, demonstrated that the 3-element Yagi-Uda array of 1.5λ GSDs is able to provide a maximum gain of 11.8dB; but did not mention the associated FBR. Chen, Jen, and Zhang, [10], considered the problem of optimizing the performance of Yagi-Uda arrays of GSDs, for low sidelobe levels of the radiation zone field patterns. Results presented in [10], for a 6-element array, suggest that low side lobe levels can only be achieved at the expense of directivity. For example, when the array's Front-to-Back Ratio (FBR) assumed a value of close to 41dB, the corresponding directivity was as low as 1.35dB. The configuration of an array of GSDs described in [11] utilized an analytical procedure involving "smooth controlled step functions", to prescribe optimum dimensions for the array's director and reflector elements. Simulation results reported therein, for antenna performance parameters, include a maximum directivity of 11.3dBi, minimum side lobe level of -10.6dB, and a maximum front to back ratio of 18.7dB: for an antenna, whose 'overall length' was given as 0.75λ at the operating frequency of 904MHz.

As implicitly noted in [12], the 3-element Yagi-Uda array of GSDs (also referred to as the "Landstorfer antenna", [13], [14]), and its variants, offer an inexpensive alternative to the classical approach of increasing the gain of Yagi-Uda arrays of straight dipoles. However, the results reported in [10], for example, suggest these arrays provide maximum gain by trading-off FBR. In some applications, such as military manpack radio [13], antennas with good directivity and FBR performances are required; and one way of enabling a good FBR performance is to locate a conducting (ground) plane behind the antenna, [15]. In the "Quasi-Landstorfer antenna" presented in [16], the reflector element of the Landstorfer antenna was replaced by a ground plane, so shaped as to mimic the contribution of the reflector of the original antenna, but with the main objective of significantly reducing the size of a base planar Landstorfer antenna. At the quasi-Landstorfer antenna's resonant frequency, a modest measured gain of 6.6dBi was reported, along with the impressive return loss of -42.7dBi.

As far as can be ascertained, the first (and probably only) analytical investigation of the performance features of GSDs (and their arrays) backed by finite ground plane structures, is that reported in [15]. Through the use of the image theory and Unified Theory of Diffraction (UTD) in a method of moments formulation and solution of the problem, the paper examined the effects of square ground plane size and parameters of the Gaussian distribution geometry (defined by $y = \pm A(1 - e^{-B^2/z^2})$) on maximum gain and sidelobe level (SLL). A number of interesting conclusions arising from the computational results were reported by the paper. For the single, 1.5λ Gauss-shaped dipole, and in the case of the 'backfire' mode considered, it was reported that the effects of the Gaussian parameter 'A' on gain and FBR is more pronounced than those of the parameter 'B'. The results also suggested that the influence of square-shaped ground plane size on gain is marginal, as maximum gain ranged between 13.224dB for a ground plane of side 1.5λ and 12.805dB for a ground plane of side 8.0λ . A particularly notable finding of the investigation was that "high gain and low side lobe level are contradictory": which, put in other words, implies that for the Gauss-shaped dipole backed by a square ground plane of finite size, a large value of maximum gain can only be achieved at the expense of low side lobe level, or vice-versa.

Towards a more extensive investigation of the influence of finite ground plane size and shape on the



performance features of the GSD, this paper reformulates the problem in terms of integro-differential equations for the radiation-zone electric field distributions. Candidate finite ground plane shapes considered in the paper are the square, circular, and rectangular shapes; and the optimum (in terms of maximum gain) 1.5λ Gauss dipole antenna is selected as candidate antenna. In the moment-method solution of the formulated problem, these ground planes were modeled by wire grids according to specifications given in [17], [18]. This approach, unlike the image theory (which strictly applies only for infinite ground planes), is more appropriate to ground planes of finite extent. Although the computational results obtained in this paper support the conclusion reported in [15] that high power gain is not compatible with low SLL (or high FBR), they very clearly indicate that maximum achievable gain vary significantly with finite ground plane size and shape. For example, for the square ground plane of side ranging between 1.22λ and 12.2λ , maximum gain (G) emerged as $0.76 \leq G \leq 15.81dB$, whereas, for the ground plane of circular shape for which radius ranged between 0.61λ and 6.10λ , maximum gain values obtained emerged as $2.88 \leq G \leq 15.81dB$. The analytical basis for the problem's formulation are presented in Section 2, and in Section 3, computational results obtained are presented and discussed, after the formulation's validation through comparisons with some published results. Key conclusions arising from these results are discussed in Section 4, which is the paper's concluding section.

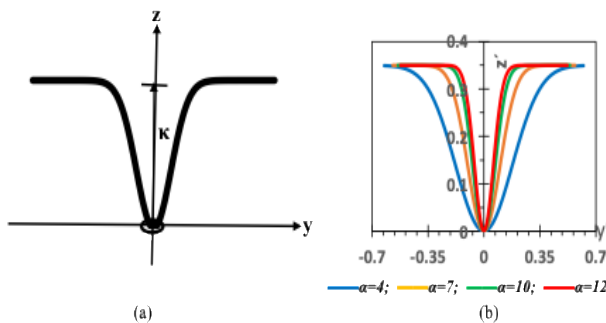


Figure 1: (a) The Gauss-shaped dipole (b) Effects of variations in Gaussian parameters

2.0 ANALYSIS

The illustration of Figure 1a describes the problem geometry for a thin-wire Gauss-shaped dipole antenna (GSDA) located on the Y – Z plane, and excited at the central point of the antenna, which corresponds to the origin of the Cartesian coordinate system. This geometry admits the analytical description given as, [15],

$$z' = \kappa \left[1 - e^{-\alpha^2 y'^2} \right] \tag{1}$$

in which the parameter κ determines the trough or depth of the Gaussian distribution and the parameter α , the degree of curvature of the arms as well as the extent of the horizontal segment of the profile. An illustration of the effects of the variations of these two parameters is provided by Figure 1b.

Clearly, therefore, this geometry can be described in terms of a position vector \vec{r}^{-T} given as:

$$\vec{r}^{-T} = y' \hat{a}_y + \kappa \left[1 - e^{-\alpha^2 y'^2} \right] \hat{a}_z \quad -y_m \leq y' \leq y_m, \tag{2}$$

provided that y_m denotes the projection of the span of the curved arm on the y-axis, and (\hat{a}_y, \hat{a}_z) are unit vectors in the y- and z- directions, respectively. Thus, the unit vector denoted by \hat{a}_u , along the dipole's axis is obtained as

$$\hat{a}_u = \frac{\hat{a}_y + 2y' \alpha^2 \kappa e^{-\alpha^2 y'^2} \hat{a}_z}{\sqrt{1 + 4\alpha^4 \kappa^2 y'^2 e^{-2\alpha^2 y'^2}}}, \tag{3}$$

and the differential element, $d\ell'$, along the axis is readily determined as

$$d\ell' = \sqrt{1 + 4\alpha^4 \kappa^2 y'^2 e^{-2\alpha^2 y'^2}} dy' \tag{4}$$

It is easy to verified that the half arm-length of the GSDA, here denoted by L, is given by

$$L = \int_0^{y_m} \sqrt{1 + 4\alpha^4 \kappa^2 y'^2 e^{-2\alpha^2 y'^2}} dy' \tag{5}$$

Accordingly, for any given numerical value of L, the GSDA parameter y_m can be determined through a solution of Equation (5). In this paper, an iterative use of the Simpson rule is adopted for the solution's associated numerical integration. In particular, following the specification of $L = 0.75\lambda$ by [1], [3], as optimum half arm length for the GSDA, this special case of interest corresponds to the numerical solution of

$$\int_0^{y_m} \sqrt{1 + 4\alpha^4 \kappa^2 y'^2 e^{-2\alpha^2 y'^2}} dy' = 0.75\lambda \tag{6}$$

With the foregoing specification of GSDA characterizing geometrical properties, a moment-method formulation commences with the following generic expression for the vector magnetic potential for a perfectly conducting thin wire, carrying the axial current $I(\ell')$;

$$\vec{A} = \frac{\mu_0}{4\pi} \int_{\ell'} \hat{a}_\ell I(\ell') \frac{e^{-jk_0 |\vec{r} - \vec{r}'|}}{|\vec{r} - \vec{r}'|} d\ell' \tag{7}$$

All parameters in Equation (7) are as defined, for example, in [17]. As is usual in antenna work, a ‘phase

approximation', for the GSDA geometry is easily obtained as

$$|\bar{r} - \tilde{r}'| = r - y' \sin \theta \sin \varphi - \kappa [1 - e^{-\alpha^2 y'^2}] \cos \theta. \quad (8)$$

so that since

$$\hat{a}_r = \sin \theta \cos \varphi \hat{a}_x + \sin \theta \sin \varphi \hat{a}_y + \cos \theta \hat{a}_z \quad (9)$$

Equation (7) passes over to

$$\bar{A} = \frac{\mu_0 e^{-jk_0 r}}{4\pi r} \int_{-y_m}^{y_m} (\hat{a}_y + 2y' \alpha^2 \kappa e^{-\alpha^2 y'^2} \hat{a}_z) I(y') e^{jk_0 (y' \sin \theta \sin \varphi + \kappa [1 - e^{-\alpha^2 y'^2}] \cos \theta)} dy', \quad (10)$$

Using the well-known relationship between vector magnetic potential and far-zone fields, it is a straightforward matter to verify that the spherical coordinates components of the radiation-zone fields, in this case, are given by

$$E_\theta = \frac{-j\omega\mu_0 e^{-jk_0 r}}{4\pi r} \int_{-y_m}^{y_m} [\cos \theta \sin \varphi - 2\sin \theta y' \alpha^2 \kappa e^{-\alpha^2 y'^2}] I(y') e^{jk_0 (y' \sin \theta \sin \varphi + \kappa [1 - e^{-\alpha^2 y'^2}] \cos \theta)} dy', \quad (11)$$

$$E_\varphi = \frac{-j\omega\mu_0 e^{-jk_0 r}}{4\pi r} \int_{-y_m}^{y_m} \cos \varphi I(y') e^{jk_0 (y' \sin \theta \sin \varphi + \kappa [1 - e^{-\alpha^2 y'^2}] \cos \theta)} dy' \quad (12)$$

According to Equation (11) and (12), in the $\varphi = 90^\circ$ (YZ) E-plane

$$E_\varphi = 0 \quad (13)$$

$$E_\theta = \frac{-j\omega\mu_0 e^{-jk_0 r}}{4\pi r} \int_{-y_m}^{y_m} [\cos \theta - 2\sin \theta y' \alpha^2 \kappa e^{-\alpha^2 y'^2}] I(y') e^{jk_0 (y' \sin \theta + \kappa [1 - e^{-\alpha^2 y'^2}] \cos \theta)} dy', \quad (14)$$

And in the orthogonal ($\varphi = 0^\circ$) H-plane,

$$E_\theta = \frac{-j\omega\mu_0 e^{-jk_0 r}}{4\pi r} \int_{-y_m}^{y_m} [2\sin \theta y' \alpha^2 \kappa e^{-\alpha^2 y'^2}] I(y') e^{jk_0 \kappa [1 - e^{-\alpha^2 y'^2}] \cos \theta} dy', \quad (15)$$

$$E_\varphi = \frac{-j\omega\mu_0 e^{-jk_0 r}}{4\pi r} \int_{-y_m}^{y_m} I(y') e^{jk_0 \kappa [1 - e^{-\alpha^2 y'^2}] \cos \theta} dy' \quad (16)$$

The MoM formulation of the problem becomes complete, when an account is provided for the finite ground plane included in the antenna structure. This account is available from the use of the wire grid model described elsewhere, [17], [18], such that the generalized MoM Ohm's law expression applicable here, admits description according to

$$\begin{bmatrix} [V_m^a] \\ [V_i^g] \end{bmatrix} = \begin{bmatrix} [Z_{mm}^{aa}] & [Z_{mj}^{ag}] \\ [Z_{in}^{ga}] & [Z_{ij}^{gg}] \end{bmatrix} \begin{bmatrix} [I_n^a] \\ [I_j^g] \end{bmatrix}, \quad (17)$$

provided that the entries into the generalized impedance matrix are prescribed by

$$\begin{bmatrix} [Z_{mm}^{aa}] & [Z_{mj}^{ag}] \\ [Z_{in}^{ga}] & [Z_{ij}^{gg}] \end{bmatrix} = \begin{bmatrix} \langle W_m^a, \mathcal{L}[T_n^a] \rangle & \langle W_m^a, \mathcal{L}[T_j^g] \rangle \\ \langle W_i^g, \mathcal{L}[T_n^a] \rangle & \langle W_i^g, \mathcal{L}[T_j^g] \rangle \end{bmatrix}, \quad (18)$$

The superscripts 'a' and 'g' in Equation (18) identify contributions to the generalized impedance matrix by the GSDA and the conducting (ground) plane elements, respectively. W_m and W_i represent

weighting functions defined on the GSDA and elements of the ground plane's wire-grid, respectively, and the corresponding expansion functions denoted respectively, by T_n and T_j are, like the weighting functions, piecewise linear functions, as described in [17] and [19]. The integro-differential linear operator symbolized by \mathcal{L} as well as inner product denoted $\langle \bullet, \bullet \rangle$, are also defined in both publications. Particulars of the wire-grid models that are of importance to the computational results, are described by Figure 2(a) and 2(b).

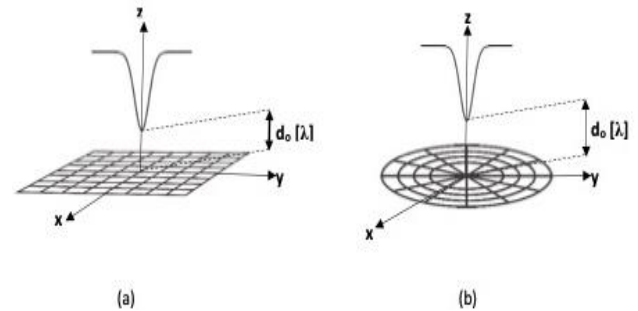


Figure 2: Illustration of the wire-grid model: (a) Rectangular ground plane (b) Circular ground plane

For Figure 2(a), nine (9) wires in either direction are utilized to form a wire grid that meets the spacing specifications of [18]. The position vector from the origin of the coordinate system to any point on an x-directed wire emerges as

$$\vec{r}_u' = x' \hat{a}_x + (n-5) \frac{L_x}{8} \hat{a}_y - d_0 \hat{a}_z, \quad -\frac{L_x}{2} \leq x' \leq \frac{L_x}{2}, \quad (19)$$

and for a y-directed grid element, as

$$\vec{r}_v' = (n-5) \frac{L_x}{8} \hat{a}_x + y' \hat{a}_y - d_0 \hat{a}_z, \quad -\frac{L_y}{2} \leq y' \leq \frac{L_y}{2} \quad (20)$$

In the case of Figure 2b, the wire-grid is formed by four (4) circular elements and twelve (12) radial elements consistent with the modelling requirements prescribed in [18]. Thus, a position vector from the origin of coordinates to a point on a typical linear grid element is given by

$$\vec{r}_e' = a_n \cos \varphi' \hat{a}_x + a_n \sin \varphi' \hat{a}_y - d_0 \hat{a}_z, \quad 0 \leq \varphi' \leq 2\pi; n=1,2,\dots,N \quad (21)$$

with

$$\vec{r}_e' = \ell' \cos \varphi_m \hat{a}_x + \ell' \sin \varphi_m \hat{a}_y - d_0 \hat{a}_z, \quad 0 \leq \ell' \leq b; m=1,2,\dots,M \quad (22)$$

being the corresponding expression for the circular grid elements.

In the foregoing expressions, a_n denotes the radius of the outermost circular element, M , the number of radial elements: φ_m the angle subtended by the m^{th} radial element on the x-axis; it is given by

$$\varphi_m = \frac{2\pi}{M}(m-1), \quad m=1,2,\dots,M, \quad (23)$$



For the purposes of specifying finite ground plane size relative to that of the GSDA, an ‘aspect ratio’ symbolized by γ is introduced and defined in Table 1.

Table 1: Ground plane size in terms of aspect ratio

Rectangular	Circular	Square
$\gamma_r = \frac{L_y/2}{y_m} = \frac{L_y}{2y_m}$	$\gamma_c = \frac{a_N}{y_m}$	$\gamma_s = \frac{L_y/2}{y_m} = \frac{L_y}{2y_m}$, $L_x = L_y$

Computational results obtained for the antenna’s performance parameters (using well-known formulas available in the literature, [3], [17], [19]) including return loss, power gain, front-to-back ratio, and directivity, are presented and discussed in Section 3.

3.0 COMPUTATIONAL RESULTS AND DISCUSSION

The computational results presented in this section refer to the $3\lambda/2$ optimum-GSDA, [1]-[4]. Here, the antenna is backed by finite ground planes of different shapes and varying sizes. First, the validity of this paper’s formulation is checked through a comparison of results obtained from the formulation’s application with a number of corresponding results available in the literature. Thereafter, the antenna’s electromagnetic response to variations in ground plane shape and size, is examined and comprehensively discussed.

3.1 Model Validation

As a check of the validity of the model developed in this paper, computational results due to the paper’s formulation are compared with corresponding results published in [3] and [15].

Table 2: Maximum gain and input admittance comparison

Normalized Radius (a/λ)	Maximum Gain (dB) [3]	Maximum Gain (dB) [Paper]	Y_{in} [3]	Y_{in} [Paper]
0.0075	6.9740	6.8173	-	0.009411 - j0.00018
0.0100	7.0740	6.8855	0.00962 - j0.00008	0.009461 + j0.0000267
0.0150	7.1320	7.0151	-	0.00956 + j0.00709

The current distribution profiles of Figure 3 display a comparison of normalized current for the optimum-shaped wire dipole antenna treated in [3] with the distribution for the same antenna, as provided by this paper’s formulation, in the absence of the ground plane. In addition to the current distribution, published gain and input admittance data available from [3] are compared in Table 2, with corresponding gain and input admittance results obtained with this paper’s model. The slight differences in the two sets of results may be attributed to the fact that the geometry of the shaped-dipole in [3], unlike the exact geometry of this paper, derived from a piecewise parabolic approximation, as well as the round-offs introduced by computation and data extraction with the use of the commercial software, ‘GETDATA’ (<https://getdata-graph-digitizer.software.informer.com>).

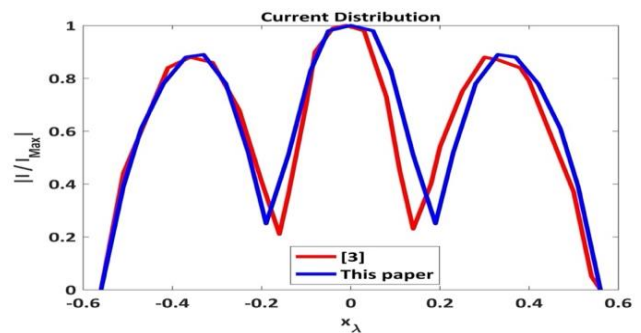


Figure 3: Comparison of the current distribution of [3, Figure 2] with corresponding results due to this paper

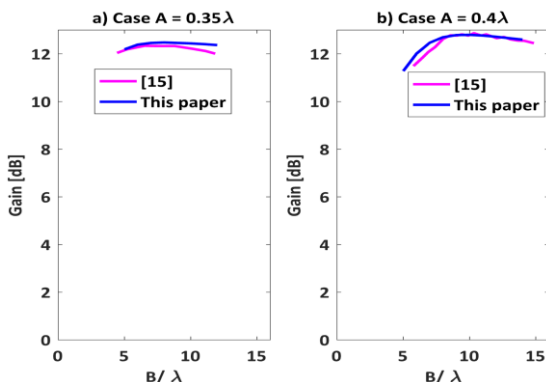


Figure 4: Comparison of variation of gain with ‘B/λ’ from [15, Figure 3] with paper’s corresponding computational results

As a further model validity check, the ‘backfire mode’ of the GSDA backed by a finite-sized square-shaped ground plane treated in [15], was selected as candidate. In this case, variations of gain with the Gaussian parameter ‘B’ of [15] (or ‘ α ’ in this paper) for fixed values of ‘A’- [15] (or ‘ κ ’-this paper) as displayed in [15, Figure 3] are compared with corresponding gain values due to this paper’s formulation. Two cases of ‘A’ (0.35λ and 0.4λ) are considered; with wire radius and square ground plane size fixed at 0.0175λ and $2\lambda \times 2\lambda$, respectively. For each combination of ‘A’ and ‘B’, the parameter ‘ y_m ’ is determined with the use of Equation (6).

The results of the comparison are displayed in Figure

4, where the close agreement between the gain profiles lend additional support to the validity of the formulation presented in Section 2.

3.2 Effects of Finite Ground Plane Shape and Size

In order to put the influence of the finite ground in proper perspective, variations of the “optimum-shaped” [3], [4], antenna’s performance metrics with the Gaussian parameters α and κ of Equation (6) are first examined using the computational results

graphically displayed in Figure 5. These results are for $2.0\lambda \leq \alpha \leq 10\lambda$ and $0.3\lambda \leq \kappa \leq 0.6\lambda$, for which y_m ranges between 0.312 ($\alpha = 10.0\lambda, \kappa = 0.6\lambda$) and 0.6990 ($\alpha = 2.0\lambda, \kappa = 0.3\lambda$). Key highlights of these results, as evident, for example, from Figure 5(a) and 5(d), include the facts that input resistance assumes its maximum value of 117Ω when $(a, \kappa) = (3.0\lambda, 0.6\lambda)$, for which y_m is 0.501λ ; and that the input reactance curves indicate that whereas there are two resonances, each for the curves for $\kappa = 0.5\lambda$ and 0.6λ , all other reactance curves exhibit one resonance only.

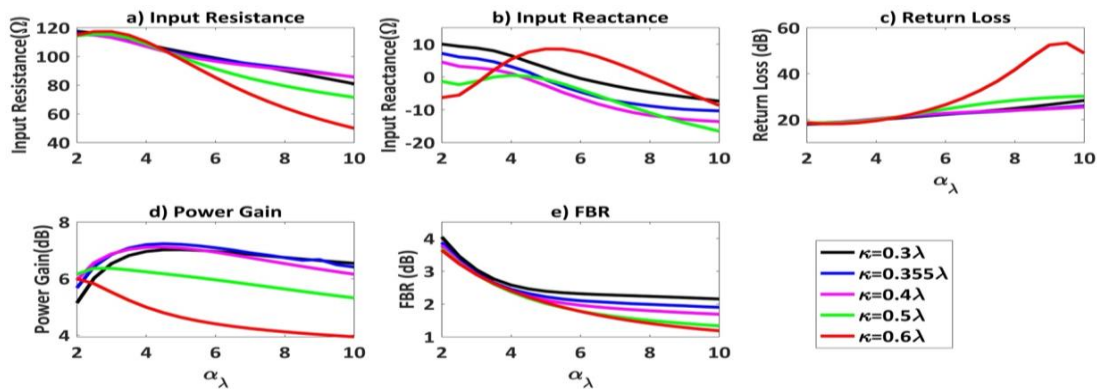


Figure 5: Variations of GSDA performance metrics with antenna parameters in the absence of a ground plane

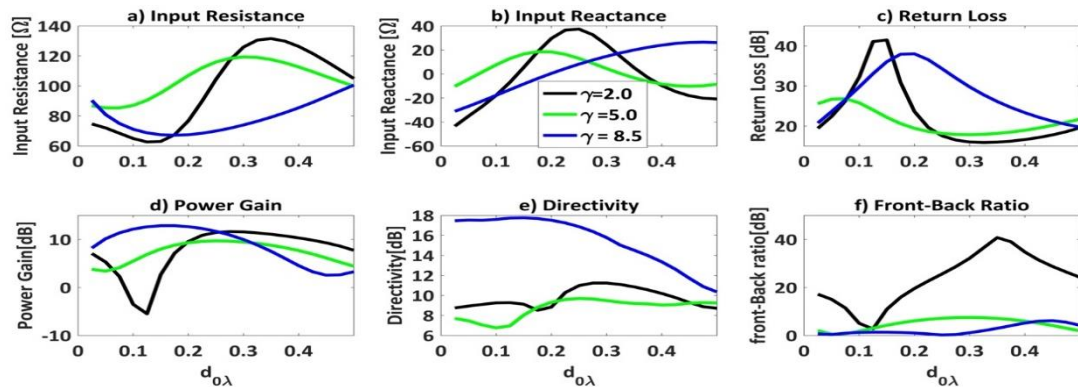


Figure 6: Variations of performance parameters of GSDA backed by a rectangular ground plane

The return loss (for a feed transmission line characteristic impedance $Z_0 = 50\Omega$) profiles of Fig. 5(c) reveal that as long as $a < 5.0\lambda$, return loss is less than 20dB, for all values of κ . Its maximum value of about 51dB is recorded, when $(a, \kappa) = (5.5\lambda, 0.6\lambda)$ that is $y_m = 0.394\lambda$. From Figure 5(e), it is seen that FBR, in general, records its maximum value when $a = 2.0\lambda$ for all the values of κ considered, and thereafter, falls in magnitude as α increases. The maximum value of FBR recorded is about 4.05dB, for the GSDA with geometry specified by $a = 2.0\lambda$ and $\kappa = 0.3\lambda$. The curves of Figure 5(d) indicate that power gain variations with the Gaussian parameters fall into two broad categories; for the first, defined by

$\kappa = 0.3\lambda, \kappa = 0.3\lambda55, \kappa = 0.4\lambda, ;$ gain (comparable in profile and magnitude) increases with α to a maximum value, before decreasing slightly to a more or less steady value. And for the set consisting of the curves for $\kappa = 0.5\lambda$ and 0.6λ , gain, whose values are generally significantly lower than those for the other set, is maximum at $\alpha = 2.0\lambda$, and thereafter, decreases monotonically. Because the maximum value of gain (7.232dB) is recorded by this GSDA when $a = 4.45\lambda$ $\kappa = 0.335\lambda$, and therefore $y_m = 0.61\lambda$. This geometry, which, by definition, [1], [3], [4] is optimum, is selected as candidate with which the influences of finite ground plane shape and size are investigated, in the ensuing discussions.



The profiles displayed in Figure 6 are for GSDA backed by a rectangular plane, for three different values of aspect ratio. It is seen from Figure 6(a) that the input resistance profiles for the cases of $\gamma = 2.0$ and $\gamma = 5.0$ are somewhat similar, although the swing for the latter is more pronounced than for the former. The resistance profile for the case $\gamma = 8.5$ differs sharply from those for the other two values of aspect ratio; and indeed, whereas minimum resistance value was recorded at about $d_0 = 0.25\lambda$ when $\gamma = 8.5$, resistance attained maximum values in this neighborhood, for the two other values of γ . More or less similar comments apply to the curves for return loss (computed for a 50Ω transmission line at the input) displayed in Figure 6(c), where maximum values of the profiles for $\gamma = 2.0$ and $\gamma = 8.5$ occurred close to $d_0 = 0.25\lambda$. A notable feature of the input reactance profiles of Figure 6(b) is that whereas two resonances were recorded for $\gamma = 2.0$ and $\gamma = 5.0$ cases, only one occurred for $\gamma = 8.5$ case. Maximum gain and maximum directivity (usually of particular interest)

occur in the descending order of $\gamma = 8.5$, $\gamma = 2.0$ and $\gamma = 5.0$, though unlike the case of maximum gain, whose values are of the same order of magnitude as can be seen from Figure 5(d), maximum directivity for the aspect ratio of 8.5 is significantly larger than for the other two values of aspect ratio. Finally, from the FBR curves of Figure 6(f), it is found that the best FBR performance is that due to $\gamma = 2.0$, and the poorest, that for $\gamma = 8.5$, with FBR for the $\gamma = 5.0$ case only slightly better.

The response of the GSDA backed by a square ground plane of varying size and for different antenna-ground plane separations is characterized by the curves displayed in Figure 7. The profiles of Figure 7(a) and 7(b) reveal that magnitudes of resistance and reactance vary approximately inversely with $d_{0\lambda}$ when aspect ratio is 8.5, with resistance values being distinctly larger than corresponding values for the other two aspect ratios, up to $d_{0\lambda}$ of about 0.4.

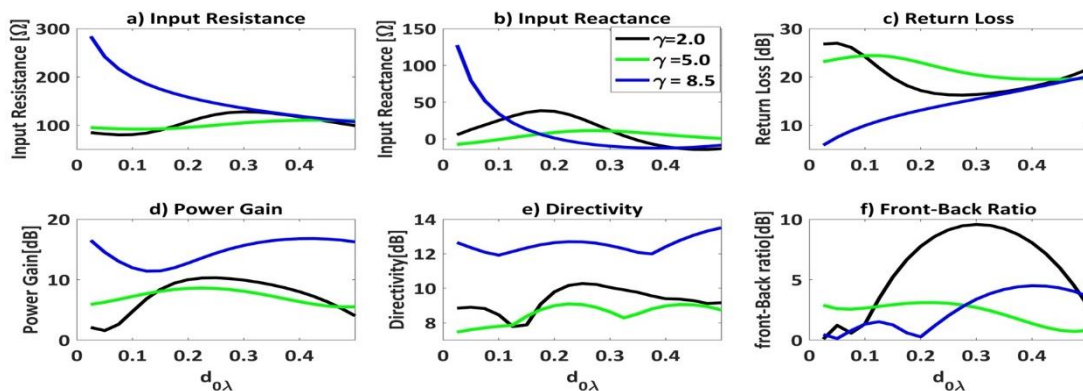


Figure 7: Profiles of performance parameters of the GSDA for the square-shaped finite ground plane case

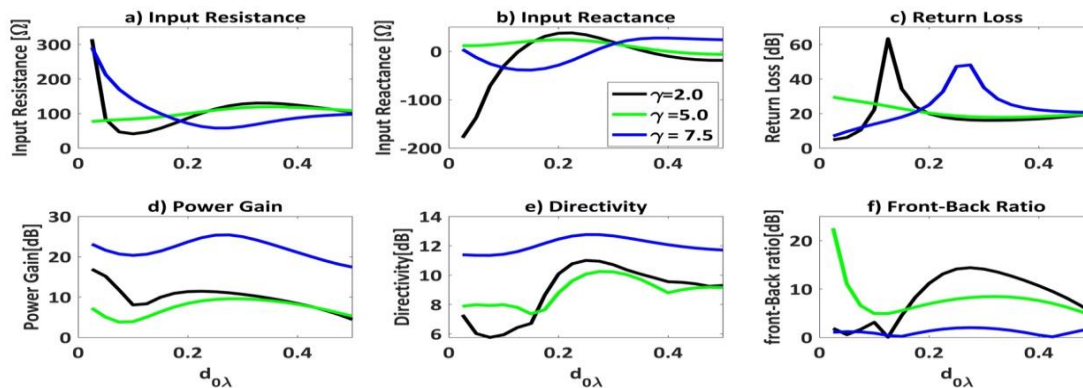


Figure 8: Influence of circular ground plane size and antenna-ground plane separation on GSDA performance parameters

It is readily observed from the reactance profile that only one resonance is featured for the three aspect ratios considered, with the occurrence of resonance being coincident at the same value of $d_{0\lambda}$ for $\gamma = 2.0$

and 5.0. On the average, and according to the curves of Figure 7(c), the best return loss performance is that recorded for the aspect ratio of 5.0; and by far the worst, that for $\gamma = 8.5$. Gain and directivity profiles

(Figure 7(d) and 7(e)) share the interesting feature that values recorded for the case of aspect ratio of 8.5 are, in both cases, greater than those for the two other aspect ratios, for all values of antenna-ground plane separation considered. And although gain values for $\gamma = 2.0$ and $\gamma = 5.0$ are comparable, on the average, directivity values for $\gamma = 2.0$ are generally better than those for $\gamma = 5.0$.

For the GSDA backed by a circularly-shaped ground plane of finite extent, variations of the performance parameters with antenna-ground plane separation and aspect ratio are described by the curves of Figure 8. Here, input resistance for a ground plane size defined by $\gamma = 8.5$, falls sharply to a minimum, before gradually increasing in value to a smaller second maximum. The input resistance profile for $\gamma = 2.0$ follows a somewhat similar pattern, though the dip from the maximum is gentler; whilst that for $\gamma = 5.0$ varies relatively insignificantly about its maximum. The input reactance profiles of Figure 8(b) reveal that unlike the reactances for ground plane size defined by $\gamma = 2.0$ and $\gamma = 8.5$, which exhibit two resonances, that for $\gamma = 5.0$ has no resonance, remaining inductive for the entire range of $d_{0\lambda}$ considered. From Figure 8(c), it is readily observed that the highest value of maximum return loss (close to 60dB) is associated with the $\gamma = 2.0$ curve, whilst those associated with $\gamma = 8.5$ and $\gamma = 5.0$, followed, in that order. It is also of interest to observe that the locus of return loss for the $\gamma = 5.0$ case does not follow the ‘notch’ response character exhibited by the profiles for the other two sizes of circular ground plane. The power gain and directivity curves of Figure 8(d) and 8(e) share the

observable feature that values recorded for the $\gamma = 8.5$ case are significantly greater than those for the $\gamma = 2.0$ and $\gamma = 5.0$ cases, over the entire range of $d_{0\lambda}$ considered in the paper. Maximum power gain emerged as about 25dB, 13dB, and 10dB for the $\gamma = 8.5$, $\gamma = 2.0$, and $\gamma = 5.0$, cases, respectively: with all of them recorded when $d_{0\lambda}$ has a value close to 0.25.

Maximum directivity values also followed the same order, emerging as approximately 13dB, 11dB, and 10dB, for the aspect ratios of 7.5, 2.0, and 5.0, respectively: and again, with all of them recorded when $d_{0\lambda}$ has a value close to 0.25. The conclusion arrived at in [15], and presented therein as “... *high gain and low sidelobe are contradictory*”, is supported by the FBR profiles of Figure 8(f). The largest value of maximum FBR, as can be seen from Figure 7(e), is that associated with the ground plane size defined by $\gamma = 5.0$, which as earlier mentioned, recorded the smallest values of maximum gain and maximum directivity. In addition, FBR for the $\gamma = 8.5$ case (for which the largest values of maximum gain and maximum directivity were recorded) emerged as the smallest among the three sets, over the span of $d_{0\lambda}$ of interest. It is worth remarking that in the neighborhood of $d_{0\lambda} = 0.25$, the value of FBR recorded for the $\gamma = 2.0$ case (which happens to be the maximum for that ground plane size) is larger than that obtained for the $\gamma = 8.5$ case.

Computational results presented in in the foregoing discussions, are rearranged in Figure 9, in order to examine the effects of ground plane shape on GSDA performance.

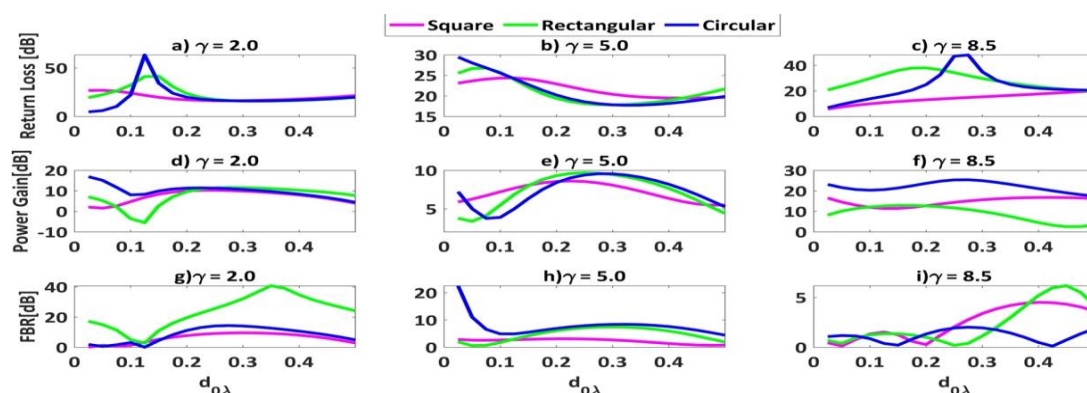


Figure 9: Representative comparisons of GSDA performance parameters for the different ground plane shapes and common values of $d_{0\lambda}$ and aspect ratio

The profiles of the first row of Figure 9(a) for return loss indicate that in terms of maximum achievable value, the circularly-shaped ground plane provides the best performance; followed by the rectangularly- and

square-shaped ground planes, in that order. Maximum achievable power gain (with profiles displayed in the second row of Figure 8 is also clearly available from the circular ground plane; however, the maximum



achievable gain from the square ground plane is larger than that from the rectangular ground plane. On the other hand, the maximum achievable FBR is, indicated by the profiles of the third row of Figure 9, is clearly provided by the rectangular ground plane case. A further demonstration of the influence of ground plane shape is provided by Figure 10, showing φ - and ϑ -components of electric field intensity due to two sets of sizes of the three candidate ground plane shapes considered in this paper.

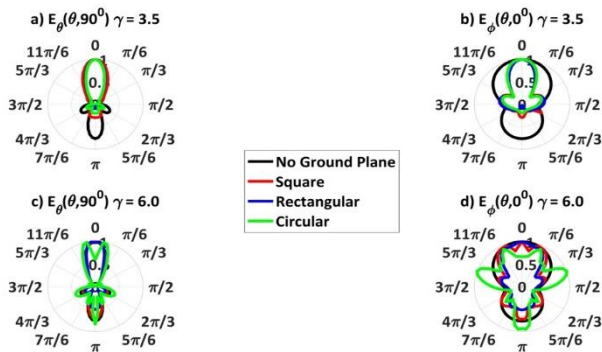


Figure 10: Influence of finite ground plane shape on far-zone electric field intensity

A comparison the metrics presented in Figure 9 with those recorded for the corresponding GSDA in the absence of a ground plane, clearly demonstrates that when the finite ground is at least 0.25λ away from the antenna, both ground plane shape and size significantly improve GSDA performance features. For example, maximum gain, which, in the absence of the ground plane assumed a value of 7.232dB, improved to 25.36dB, 19.01dB, and 15.81dB, with the respective introduction of the circular, rectangular, and square shaped ground planes. Maximum achievable FBR also improved from 4.05dB to 14.5dB, 25.61dB, and 15.62dB, respectively, following the introduction of finite ground planes with the circular, rectangular, and square shapes. It should be remarked, as suggested by the field patterns of Figure 10, that increase in relative size of ground plane beyond an aspect ratio of 4.5 attracts significant deformations in the far-zone radiation patterns.

4.0 CONCLUSION

This paper has comprehensively investigated the influence of ground plane shape and size on the performance features of the Gauss-Shaped Dipole Antenna (GSDA), which has been established in the literature as the optimum shaped wire antenna. Computational results describing the effects of finite-sized, circular, rectangular, and square ground plane shapes on GSDA performance characteristics were

presented. The results indicated that for any given shape, ground plane size, here specified in terms of an aspect ratio, significantly influenced all the GSDA performance metrics, including power gain, return loss, front-back-ratio (FBR), and directivity. As examples, for the circularly shaped ground plane, gain and FBR ranged between 2.88dB and 25.36dB and 1.94dB and 14.5 dB, respectively, as aspect ratio varied between 1.0 and 10.0. Corresponding values recorded for the square-shaped ground plane emerged as 0.76dB and 16.81dB (for gain) and 0.146dB and 15.62dB (for FBR), respectively. The influence of size is exemplified by the fact that maximum gain for the circular-, rectangular-, and square-shaped ground planes were recorded for the respective aspect ratios of 7.5, 8.0, and 10.0. Interestingly, minimum values of gain for these shapes of ground plane occurred for the comparable sizes specified by the respective aspect ratios of 6.0, 7.5, and 8.0. It is important to remark that the foregoing results were recorded for antenna-ground plane separations of 0.25λ . The computational results are consistent with the conclusion in the literature that for the GSDA backed by a finite-sized ground plane high values of maximum achievable gain can only be obtained at the expense of front-to-back ratio.

Finally, one possible extension of this paper’s presentation may be offered by an exploration of the performance of a sparse randomly spaced array of the GSDA, backed by a finite ground plane, when subjected to optimization as described in [20].

REFERENCES

- [1] Landstorfer, F. "A new type of directional antenna," *1976 Antennas and Propagation Society International Symposium, Amherst, MA, USA, 1976*, pp. 169-172, doi: 10.1109/APS.1976.1147636
- [2] Chen, Y. et al., "Landstorfer Printed Log-Periodic Dipole Array Antenna With Enhanced Stable High Gain for 5G Communication," *in IEEE Transactions on Antennas and Propagation*, vol. 69, no. 12, pp. 8407-8414, Dec. 2021, doi: 10.1109/TAP.2021.3090079
- [3] Cheng, D. K., and Liang, C. H. "Shaped wire antenna with maximum directivity," *Electronics Letters*, vol. 18, issue 19. pp. 816-818, 1982, doi: 10.1049/el.19820555.
- [4] Wang, J. H. and Lang, R. "Directivity optimization of curved surface dipole antennas," *J. of Electron. (China)* 11, 1994. pp. 322–331 doi: 10.1007/BF02778386
- [5] Kataja, J. "On shape optimization of wire dipole antennas," *2010 URSI International*

- Symposium on Electromagnetic Theory, Berlin, Germany, 2010*, pp. 269-271, doi: 10.1109/URSI-EMTS.2010.5636982.
- [6] Kataja, J. "Shape optimization for curved dipole antennas," *URSI Finnish XXXI Convention on Radio Science and Electromagnetics 2008 Meeting, Espoo, Finland*, pp. 67-68.
- [7] Toivanen, J. I., Makinen, R. A. E., Jarvenpaa, S., Yla-Oijala, P., and Rahola, J. "Electromagnetic Sensitivity Analysis and Shape Optimization Using Method of Moments and Automatic Differentiation," *in IEEE Transactions on Antennas and Propagation*, vol. 57, no. 1, pp. 168-175, 2009, doi: 10.1109/TAP.2008.2009657.
- [8] Wang, J. H., Jen, L., and Jian, S. S. "Optimization of the dipole shapes for maximum peak values of the radiating pulse," *IEEE Antennas and Propagation Society International Symposium 1997*. Digest, Montreal, QC, Canada, 1997, pp. 526-529 vol.1, doi: 10.1109/APS.1997.630214.
- [9] Liang, C. H. and Cheng, D. "Directivity optimization for Yagi-Uda arrays of shaped dipoles," *in IEEE Transactions on Antennas and Propagation*, vol. 31, no. 3, pp. 522-525, May 1983, doi: 10.1109/TAP.1983.1143085.
- [10] Chen, W., Jen, L., and Zhang, S. M. "Radiation pattern optimisation for Yagi-Uda arrays of shaped dipole antennas", *Electronics Letters*, vol 30, issue 16 1994. pp. 1264-1265 doi: 10.1049/el:19940877.
- [11] Narváez, A.R., Molina, H.B. "Landstorfer Antenna Structure Shaping Based on Parameterized Parallel Curves", 2024, In: Olmedo Cifuentes, G.F., Arcos Avilés, D.G., Lara Padilla, H.V. (eds) *Emerging Research in Intelligent Systems. CIT 2023. Lecture Notes in Networks and Systems*, vol 902. Springer, Cham. https://doi.org/10.1007/978-3-031-52255-0_5
- [12] Chen, Y. et al., "Gain Enhancement for Landstorfer Yagi Antenna Using Zero- Index Metamaterials," *2020 IEEE MTT-S International Wireless Symposium (IWS)*, Shanghai, China, 2020, pp. 1-3, doi: 10.1109/IWS49314.2020.9359970
- [13] Breakall, J. K., Rohde, U. L., and Poddar, A. K. "A look at a novel curved antenna design with FEKO," *2023 International Applied Computational Electromagnetics Society Symposium (ACES), Monterey/Seaside, CA, USA, 2023*, pp. 1-2, doi: 10.23919/ACES57841.2023.10114703.
- [14] Mak, A. C. K., Rowell, C. R., and Murch, R. D. "Low Cost Reconfigurable Landstorfer Planar Antenna Array," *in IEEE Transactions on Antennas and Propagation*, vol. 57, no. 10, pp. 3051-3061, 2009, doi: 10.1109/TAP.2009.2028593.
- [15] Wang, J. H., and Jen, L. "Analysis of curvilinear dipoles and their arrays with finite reflectors," *Proceedings of IEEE Antennas and Propagation Society International Symposium and URSI National Radio Science Meeting, Seattle, WA, USA, 1994*, pp. 1002-1006 vol.2, doi: 10.1109/APS.1994.407919
- [16] Aziz, M. A. Roy, S., and Braaten, B. D. "A New Printed Quasi-Landstorfer Antenna," *in IEEE Transactions on Antennas and Propagation*, vol. 60, no. 5, pp. 2531-2536, 2012, doi: 10.1109/TAP.2012.2189930.
- [17] Ayorinde, A. A., Adekola, S. A., and Ike Mowete, "Performance characteristics of loop antenna above a ground plane of finite extent", *Proceedings of Progress in Electromagnetics Research Symposium (PIERS), Taipei, 2013*. pp.769-774
- [18] Alhaj Hasan, A., Kvasnikov, A. A., Klyukin, D.V., Ivanov, A. A., Demakov, A. V., Mochalov, D. M., and Kuksenko, S. P. "On Modeling Antennas Using MoM-Based Algorithms: Wire-Grid versus Surface Triangulation". *Algorithms*. 2023; 16(4):200. <https://doi.org/10.3390/a16040200>
- [19] Ayorinde, A. A., Adekola, S. A., and Ike Mowete, "Logarithmically-Wound Helix Antenna Excited for Axial-Mode Operations" *Jordan Journal of Electrical Engineering*, vol. 7, no. 3, pp. 265-287, 2021, doi: 10.5455/jjee.204-1614026886
- [20] Mustapha, S. A., Sani, S.M., and Abu-Bilal, K. A. "Optimization of Sparse Randomly Spaced Linear Antenna Array using Hybrid Iteratively Reweighted Least Squares", *Nigerian Journal of Technology* vol. 40, No. 2, 2021, 2021, pp. 302-307. doi: <http://dx.doi.org/10.4314/njt.v40i2.16>

